NANO LETTERS

2008
Vol. 8, No. 8
2265-2270

Multiple Surface Plasmon Modes for a Colloidal Solution of Nanoporous Gold Nanorods and Their Comparison to Smooth Gold Nanorods

Hye-Mi Bok,[†] Kevin L. Shuford,[§] Sungwan Kim,[†] Seong Kyu Kim,[†] and Sungho Park*[,†,‡]

Department of Chemistry, BK21 School of Chemical Materials Science and SKKU Advanced Institute of Nanotechnology, Sungkyunkwan University, Suwon 440-746, South Korea, and Chemical Sciences Division, Oak Ridge National Laboratory, P.O. Box 2008 MS6142, Oak Ridge, Tennessee 37831

Received April 1, 2008; Revised Manuscript Received May 27, 2008

ABSTRACT

The paper represents a novel approach to investigating localized surface plasmon (LSP) resonance modes of nanoporous Au nanorods (NRs) in a solution phase with control over surface morphology. Au NRs, which have distinctive features such as nanopores and ligaments, showed interesting LSP resonance modes depending on the surface morphology and the total length of the structure. Compared with the analogous smooth surface NRs, the LSP modes of nanoporous NRs are red-shifted, which can be interpreted as a longer effective rod length and larger amplitude of plasmon oscillation.

The photoexcitation of loosely bound electrons on a metal surface is called a surface plasmon polariton for planar surfaces or a localized surface plasmon (LSP) resonance for nanometer-sized metallic structures.[1–9] The LSP condition depends on the size, shape, composition, environment, and the dielectric constant of the metal. The characterization and utilization of LSP resonances in spherical particles has been at the center of nanophotonics due to their fundamental importance as standard materials. Now one can easily synthesize spherical, metal nanoparticles with a fine controllability over a broad range of size regimes. Even large aspect ratio nanoparticles, such as nanorods (NRs), can be readily synthesized through a wet-chemical synthetic route or template-assisted methods.[10–13] Because NRs have an anisotropic shape, they support more complicated LSP modes than spherical nanoparticles. For example, small NRs display dipolar LSP resonances that oscillate along both the short and long axes, which are known as transverse and longitudinal modes, respectively.[14–16] However, when the length becomes significantly larger than the diameter, higher-order longitudinal modes appear as a result of the dephasing (or retardation) of the field within the NRs.[14–16] Multipole LSP resonances are of fundamental interest and are important for applications related to near-field or far-field imaging and sensing. Here we report the first experimental observation of multipole LSP modes for colloidal, Au NRs with a nanoporous surface structure. The optical properties vary as a function of length as well as the surface roughness. Compared with the analogous smooth surface NRs, the LSP modes of nanoporous NRs are red-shifted, which can be interpreted as a longer effective rod length and larger amplitude of plasmon oscillation.

Our strategy for generating nanoporous Au NRs employs the electrochemical codeposition of Au/Ag alloy materials into the pores of anodized aluminum oxide (AAO) templates and the subsequent etching of Ag from the alloy structure (Figure 1). Preferential dissolution of the less noble component (Ag) of the alloy results in the formation of nanoporous Au structures due to an intrinsic dynamic pattern formation process, in which the more noble metal (Au) atoms tend to aggregate into two-dimensional clusters through a phase separation process at the solid−acid interface.[17,18] Monitoring the charge passed during the electrochemical deposition step can control the length of the NRs. The surface morphology can be controlled by tailoring the ratio of the Au_x/Ag_{1-x} alloy composition. When x is 1, pure Au NRs

* To whom correspondence should be addressed. E-mail: spark72@skku.edu. Fax: 82-31-290-7075.
† Department of Chemistry, BK21 School of Chemical Materials Science, Sungkyunkwan University.
‡ SKKU Advanced Institute of Nanotechnology, Sungkyunkwan University.
§ Oak Ridge National Laboratory.

10.1021/nl800924r CCC: $40.75
Published on Web 07/08/2008

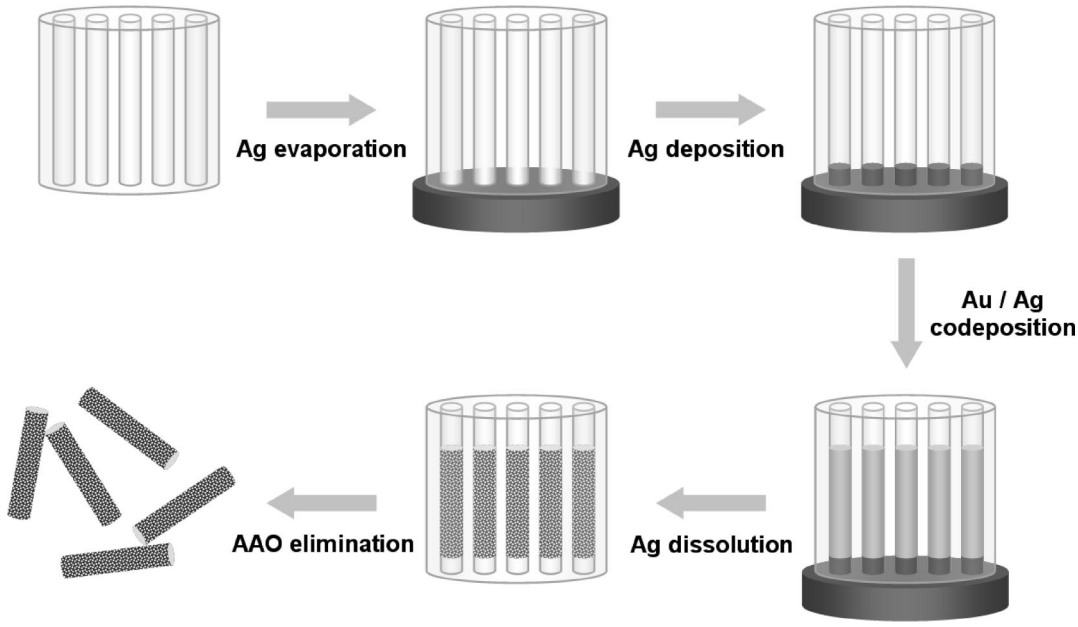

Figure 1. Schematic representation of the synthesis of nanoporous Au NRs. The electrochemical codeposition of Au/Ag results in alloy NRs in the interior of AAO templates. The Ag component was dissolved with concentrated nitric acid and the resulting nanoporous Au NRs were formed.

with a smooth surface are generated. The NR diameter depends on the pore diameter of the AAO template utilized, and here templates with a pore diameter of 85 ± 5 nm have been used. In this size regime, the 1D nanostructures exhibit higher-order, longitudinal LSP resonances as well as a transverse dipole mode.[16]

Typical field-emission scanning electron microscopy (FESEM) images of the resulting Au NRs reveal their narrow size distribution and homogeneous morphology (Figure 2). When the molar ratio of Au is 1, Au NRs with a smooth wall surface are obtained. The high-resolution FESEM image shows the smooth surface and the corresponding transmission electron microscopy (TEM) image reveals a featureless morphology (Figure 2A). The length and diameter are 404 (±35) nm and 85 (±4) nm, respectively. As expected, the corresponding visible−near IR extinction spectrum shows a transverse LSP mode appearing at 552 nm (Figure 2D, spectrum a). The longitudinal dipole mode and a higher-order mode appear at 1754 and 810 nm, respectively. These wavelengths are in good agreement with the values reported in the literature.[16] When the molar ratio of Au in the Au_x/Ag_{1-x} alloy composition is 0.50, selective etching of Ag results in nanoporous, Au NRs as shown in Figure 2B. The length and diameter are 398 (±18) nm and 83 (±5) nm, respectively. Their pore diameter is 15 (±3) nm and the ligament size is 22 (±4) nm. Herein, the "ligament" indicates the Au "bone" structure after Ag dissolution. The TEM image reveals nanoporous features that are in contrast to the analogous Au NRs with smooth walls. Their corresponding extinction spectrum is displayed in Figure 2D, spectrum b. The distinct features are the red-shift of both transverse and longitudinal LSP modes compared to the smooth NRs. The magnitude of the red-shift becomes even larger as the surface roughness increases, as shown in Figure 2D, spectrum c. Spectrum c was obtained from the sample represented in Figure 2C. The preferential etching of the Ag component from the Au_x/Ag_{1-x} alloy NR ($x \sim 0.36$) results in nanoporous Au NRs with a pore diameter of 7 (±2) nm and a ligament size of 14 (±3) nm. As is clearly evident in the high-resolution FESEM and TEM images, the nanopores are evenly distributed over the whole structure (Figure 2C). Although the physical dimensions for length and diameter are comparable to other NRs shown in Figure 2, all of the LSP resonances are significantly red-shifted. As a comparison, a spectrum for Au_x/Ag_{1-x} alloy NRs ($x \sim 0.50$ without Ag etching) with the similar size is plotted with a red solid line. The transverse LSP mode red-shifted, while the longitudinal LSP modes appear at the similar wavelengths as in the case of pure smooth Au NRs.

One discernible feature with the sample in Figure 2C is the longer ligament pathway from one side to the other side. When the surface is smooth, the loosely bound surface electrons can oscillate along the length of NR diameter. However, when the surface is corrugated, the effective oscillation length is longer than the NR diameter. The increase of effective oscillation length will result in the red-shift of LSP modes. This is clearly evident in the spectra shown in Figure 2D. Another noticeable feature is the band broadening with nanoporous NRs compared to smooth NRs, which can be ascribed to the disordered distribution of pores and ligaments. It is expected that the disorderedness of such features will generate a broad distribution of effective oscillation path lengths. Therefore their apparent NR size for electron oscillation will be larger than the case with smooth NRs. For example, the longitudinal LSP modes for nanoporous NRs when $L \sim 420$ nm match the corresponding LSP modes of smooth NRs when $L \sim 560$ nm. The irregular surface morphology originating from nanopores and ligaments leads to the longer average oscillation pathways. The other possible explanation for the observed red-shift is related

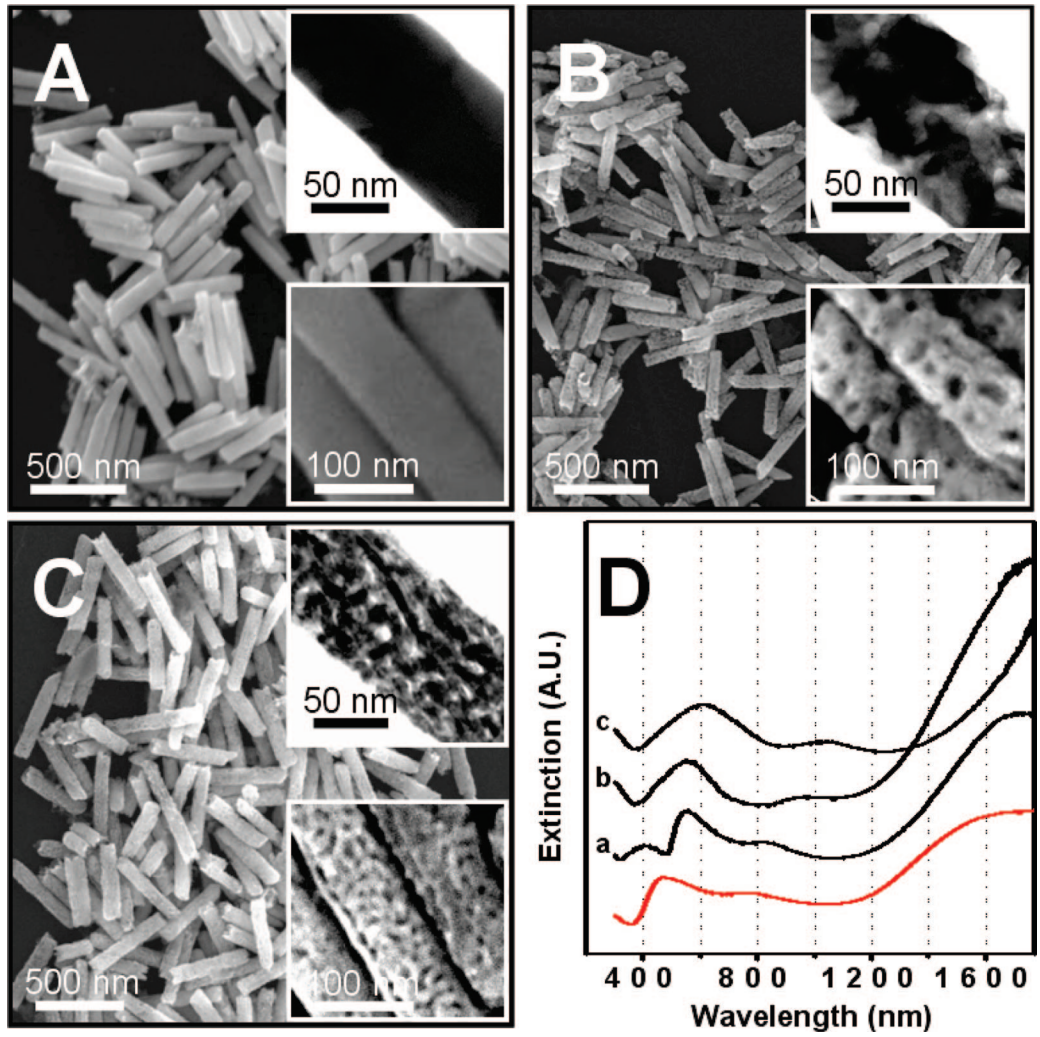

Figure 2. FESEM images of (A) smooth Au NRs ($L = 404$ (± 35) nm and $d = 85$ (± 4) nm), (B) nanoporous Au NRs ($L = 398$ (± 18) nm and $d = 83$ (± 5) nm) prepared from the dissolution of Ag from Au_x/Ag_{1-x} alloy NRs ($x \sim 0.50$), and (C) nanoporous Au NRs ($L = 420$ (± 18) nm and $d = 82$ (± 6) nm) prepared from the dissolution of Ag from Au_x/Ag_{1-x} alloy NRs ($x \sim 0.36$). (D) Visible-near IR extinction spectra for sample (A), (B), and (C) corresponding to spectrum (a), (b), and (c), respectively. The red-solid line is the spectrum for Au_x/Ag_{1-x} alloy NRs ($x \sim 0.50$ without Ag etching $L = 400$ (± 18) nm and $d = 85$ (± 4) nm). All the spectra are measured in D_2O. Insets are the corresponding zoom-in TEM (upper) and FESEM (lower) images.

to the plasmon electron density. A model based on the Drude model can explain the red-shift of nanoporous Au NRs in which the Au LSP modes red-shift due to a decrease in electron density. In the previously reported paper, the effect of electron density variation in Au NRs was considered by the Drude model, and they observed the good agreement between the theory and the experimental results.[19] When the electron density changes, the band position changes but there is little change in bandwidth.[19] However, our experimental results show that both the band position and the bandwidth change as a function of the porosity. The increase of effective length and the inhomogeneous distribution of such path-lengths in a nanoporous Au NRs are the possible explanation for the observed band-shift and band-broadening.

We synthesized nanoporous, Au NRs (selective etching of Ag from Au_x/Ag_{1-x} alloy NR when $x \sim 0.36$) with different lengths ranging from ca. 180 to 624 nm and measured their corresponding visible-near IR extinction spectra (Figure 4A). FESEM images reveal their narrow size distribution and homogeneous morphology (Figure 3). As with smooth Au NRs, the transverse modes at ~550−650 nm are largely insensitive to the increasing aspect ratio; however, the longitudinal dipole modes red-shift considerably from 1290 nm for $L \sim 180$ nm well into the IR for $L > 420$ nm. One noticeable feature is the appearance of discernible peaks between 1036 and 1400 nm, which correspond to quadrupole LSP resonances, when the rod length exceeds ca. 400 nm. The peak initially at 1036 nm (Figure 4A, spectrum d) shifts toward longer wavelengths as the length increases to 624 nm. Similar red-shifts have been observed previously in lithographically generated patterns and in a colloidal suspension of Au NRs.[14,16] We plotted the observed LSP resonances of nanoporous, Au NRs as a function of total NR lengths (Figure 4B, filled symbols). As a direct comparison, the corresponding Au NRs with smooth surfaces are plotted with open symbols. The nanoporous structure induces significantly larger red-shifts in longitudinal modes than in transverse modes. For example, when the NR length is ca. 250 nm, the transverse mode at 542 nm is slightly shifted to 598 nm, while the longitudinal mode at 1180 nm

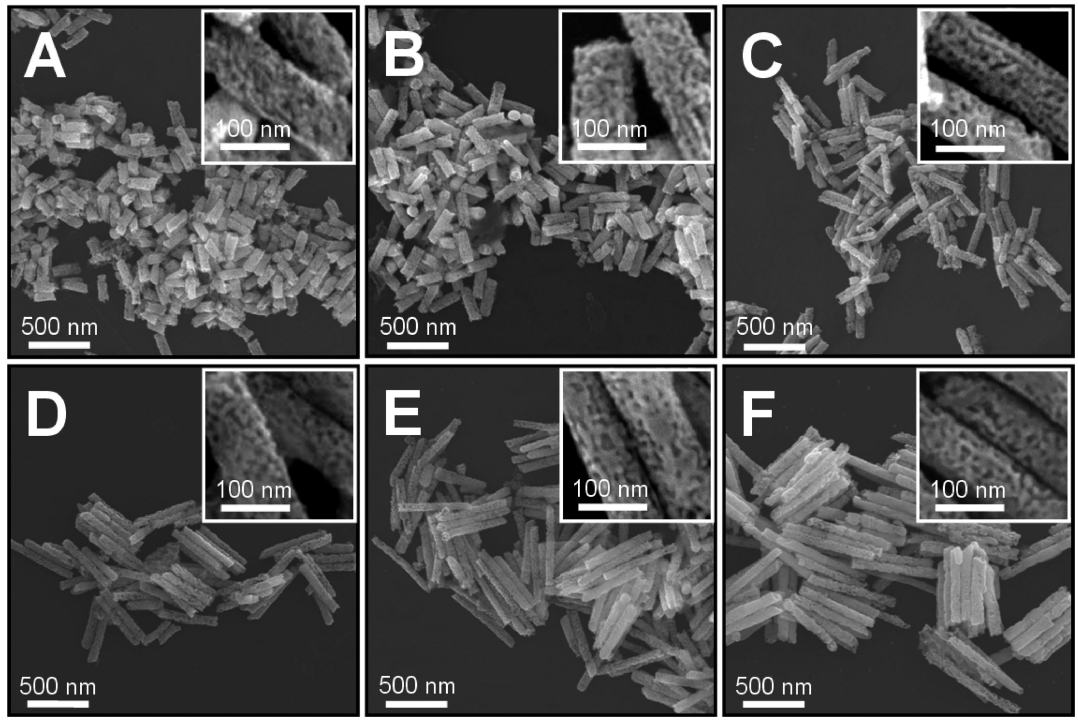

Figure 3. FESEM images of nanoporous Au NRs with different lengths ($L \approx$ (A) 180, (B) 250, (C) 304, (D) 460, (E) 560, and (F) 624 nm). Insets are the corresponding zoom-in images.

moves out to 1480 nm. Another noticeable feature is the wavelength shift as the NR length increases. While the transverse dipole modes for both smooth and nanoporous NRs have a negligible slope (squares in Figure 4B), the longitudinal LSP modes have slopes of 2.8 for dipole modes and 1.7 for quadrupole modes. The decrease of slope for higher-order modes is in good agreement with previous results.[14,16,20] A good linear fit (R^2 values of ca. 0.99) provides equations for predicting where the plasmon modes will appear under these experimental conditions.

We have calculated the optical properties of the Au NRs with both smooth and nanoporous surfaces using the discrete dipole approximation (DDA).[21,22] Detailed descriptions of DDA have been published numerous times in the nanophotonic literature, and therefore we only provide the salient points of the method here. The particle is represented by an array of point dipoles. Each dipole obtains a polarization from the local field at that site, which has contributions from the incident field and the fields radiated from all of the other dipoles in the array. The polarizability of each dipole incorporates the optical constants of Au[23] and is assigned based on a lattice dispersion relation.[24] The set of coupled dipole equations are formulated into a large, dense matrix equation that is solved iteratively for the induced polarization at each site. The polarizations are then used to calculate the nanoparticle extinction via the optical theorem.

The nanoporous structures used in the calculations have been generated by randomly removing dipoles from smooth cylindrical geometries, which are initially 80 nm in diameter and various lengths that correspond to the experimental NRs. Only lattice sites within three layers of the particle surface were allowed to be removed. This distance is approximately the same size as the surface features present on the nanoporous NRs investigated experimentally. A preliminary investigation (not shown here) determined that the largest red-shifts in the spectral peaks were produced when half of the eligible dipoles were removed. Removing either more or less than half of the "surface" dipoles generates a structure that is smoother and leads to peaks that are red-shifted less. All of the simulation results presented on nanoporous NRs use this prescription for generating the structures.

Figure 4C displays the optical spectra of nanoporous NRs of various lengths ranging from 180 to 620 nm. These results agree well with the experimentally measured spectra (panel A) and show the same major trends. As the rods get longer, the peaks associated with longitudinal plasmon modes ($\lambda >$ 700 nm) become more intense and shift to longer wavelengths. As observed experimentally, the transverse LSP resonance located at ~550 nm is largely insensitive to increasing the rod length. Figure 4D displays the local maxima of the extinction spectra as a function of rod length for nanoporous (filled symbols) and smooth NRs (open symbols). The corresponding experimental plot is shown in panel B. The agreement between theory and experiment is especially good when the plasmon resonances are well resolved, whereas the calculations are typically shifted from experiment when the LSP resonances are just beginning to emerge. For example, the nanoporous data points for the longitudinal dipole (filled circles) and quadrupole (filled triangles) at the end of each series agree well, but the theoretical data points at the beginning of each series are blue-shifted from the corresponding experimental data points. For smooth rods a similar situation occurs, but the shift is to longer wavelengths instead of shorter ones. Theory also predicts some longitudinal resonances that the experiment is unable to resolve as is indicated by the additional data

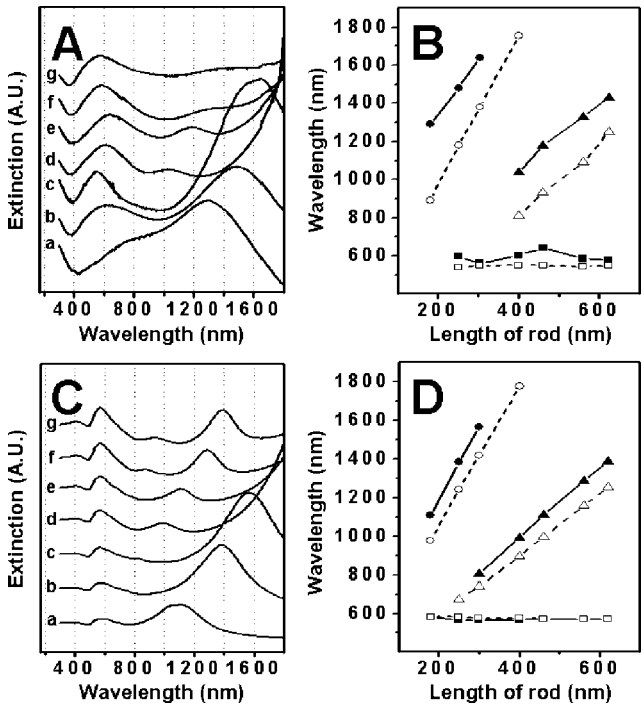

Figure 4. (A) Experimental visible-near IR extinction spectra of (a) 180, (b) 250, (c) 304, (d) 420, (e) 460, (f) 560, and (g) 624 nm long nanoporous Au NRs in D_2O. (B) Plot of LSP modes versus length of nanoporous NRs (filled symbols) and smooth NRs (open symbols). The squares, circles, and triangles correspond to transverse dipole, longitudinal dipole, and longitudinal quadrupole modes, respectively. (C) Simulated extinction spectra of (a) 180, (b) 250, (c) 300, (d) 400, (e) 460, (f) 560, and (g) 620 nm long nanoporous Au NRs. (D) Calculated extinction maxima as a function of NR length using the same labeling convention as panel B.

points for the quadrupole mode in both smooth and nanoporous structures.

The calculations and experiment both indicate that the nanoporous surface structure induces red-shifts in the LSP resonances (Figure 4B,D). The highly nanoporous NRs have a significantly larger surface area that promotes enhanced electromagnetic fields at the interstices. The field enhancement is similar to the junction effect that occurs between two nanoparticles in close proximity to one another but on a finer scale. It has been shown that the build-up of large field-induced polarization shifts the LSP peaks in the optical spectrum to longer wavelengths and that removing the spatial regions where polarization builds up (smoothing the surface) leads to blue-shifts in the LSP peaks.[25–27] These findings are consistent with the experimental and theoretical data presented here. Physically, the pores and ligaments make it easier for the NRs to polarize. This leads to red-shifts in the LSP peaks compared to smooth NRs and can be interpreted as an increase in effective rod length. In addition to red-shifts, we also find that the nanoporous structure broadens the resonance widths and obscures some of the fine structure observed in the spectra of smooth NRs (Supporting Information, Figure S1). The larger widths suggest an increase in the radiative damping rate and a decrease in the coherent lifetimes of the LSP modes. Apparently, the nanoporous structure generates more complex plasmon excitations over a broader distribution of oscillator frequencies that lead to a faster decay of LSP resonances.

In conclusion we have observed transverse and longitudinal LSP resonances including higher-order modes in colloidal suspension of nanoporous, Au NRs. It has been shown that one can systematically synthesize different surface morphology on NRs by controlling the molar ratio of two different metals and the subsequent dealloying process. When the physical size of nanoporous NRs is comparable to those of smooth NRs, the LSP modes of the former are red-shifted from those of the latter. In this context, we have introduced a new class of materials for optical devices. These nanostructures highlight the importance of tunability via surface morphology (especially using nanopores and ligaments) for the ultimate control of optical properties of nanostructures. Nanoporous NRs are expected to show strong near-field profiles, which are important for near-field imaging and surface enhanced Raman scattering (SERS). Also, the high surface-to-total-volume ratio will allow one to develop more sensitive sensor applications after modifying the surface of nanoporous NRs such as antibodies, given that the chemical environmental change will affect more on the LSP resonances of nanoporous NRs compared to smooth NRs. These applications are currently being studied and will be reported in the future.

Acknowledgment. This work was supported by the Korea Research Foundation Grant funded by the Korean Government (MOEHRD, KRF-2005-005-J11902 and KRF-C00050) and the Korea Science and Engineering Foundation (R01-2006-000-10426-0-2006). S.K.K. thanks the KOSEF-SRC program (Center for Nanotubes and Nanostructured Composites). K.L.S. was supported by the Wigner Fellowship Program and the Division of Chemical Sciences, Biosciences, and Geosciences, Office of Basic Energy Sciences, U.S. Department of Energy under Contract DE-AC05-00OR22725 with Oak Ridge National Laboratory, managed and operated by UT-Battelle, LLC.

Supporting Information Available: DDA calculations of solid, Au NRs, and experimental details. This material is available free of charge via the Internet at http://pubs.acs.org.

References

(1) Barnes, W. L.; Dereux, A.; Ebbesen, T. W. *Nature* **2003**, *424*, 824.
(2) Oldenburg, S. J.; Jackson, J. B.; Westcott, S. L.; Halas, N. J. *Appl. Phys. Lett.* **1999**, *75*, 2897.
(3) Kumbhar, A. S.; Kinnan, M. K.; Chumanov, G. *J. Am. Chem. Soc.* **2005**, *127*, 12444.
(4) Jin, R.; Cao, Y.; Mirkin, C. A.; Kelly, K. L.; Schatz, G. C.; Zheng, J. G. *Science* **2001**, *294*, 1901.
(5) Millstone, J. E.; Park, S.; Shuford, K. L.; Qin, L.; Schatz, G. C.; Mirkin, C. A. *J. Am. Chem. Soc.* **2005**, *127*, 5312.
(6) Jana, N. R.; Gearheart, L.; Murphy, C. J. *J. Phys. Chem. B* **2001**, *105*, 4065.
(7) Kim, F.; Song, J. H.; Yang, P. *J. Am. Chem. Soc.* **2002**, *124*, 14316.
(8) Ung, T.; Liz-Marzan, L. M.; Mulvaney, P. *J. Phys. Chem. B* **2001**, *105*, 3441.
(9) Martin, C. R. *Science* **1994**, *266*, 1961.
(10) Li, T.; Hunyadi, S. E.; Gou, L.; Gao, J.; Orendorff, C. J.; Gole, A. M.; Sau, T.; Murphy, C. J. *J. Phys. Chem. B* **2005**, *109*, 13857.
(11) Park, S.; Lim, J.-H.; Chung, S.-W.; Mirkin, C. A. *Science* **2004**, *303*, 348.

(12) Nicewarner-Peña, S. R.; Freeman, R. G.; Reiss, B. D.; He, L.; Peña, D. J.; Walton, I. D.; Cromer, R.; Keating, C. D.; Natan, M. J. *Science* **2001**, *294*, 137.
(13) Kovtyukhova, N. I.; Martin, B. R.; Mbindyo, J. K. N.; Smith, P. A.; Razavi, B.; Mayer, T. S.; Mallouk, T. E. *J. Phys. Chem. B* **2001**, *105*, 8762.
(14) Krenn, J. R.; Schider, G.; Rechberger, W.; Lamprecht, B.; Leitner, A.; Aussenegg, F. R.; Weeber, J. C. *Appl. Phys. Lett.* **2000**, *77*, 3379.
(15) Laurent, G.; Felidj, N.; Aubard, J.; Levi, G.; Krenn, J. R.; Hohenau, A.; Schider, G.; Leitner, A.; Aussenegg, F. R. *J. Chem. Phys.* **2005**, *122*, 011102.
(16) Payne, E. K.; Shuford, K. L.; Park, S.; Schatz, G. C.; Mirkin, C. A. *J. Phys. Chem. B* **2006**, *110*, 2150.
(17) Erlebacher, J.; Aziz, M. J.; Karma, A.; Dimitrov, N.; Sieradzki, K. *Nature* **2001**, *410*, 450.
(18) Ji, C.; Searson, P. C. *J. Phys. Chem. B* **2003**, *107*, 4494.
(19) Mulvaney, P.; Perez-Juste, J.; Giersig, M.; Liz-Marzan, L. M.; Pecharroman, C. *Plasmonics* **2006**, *1*, 61.
(20) Kim, S.; Shuford, K. L.; Bok, H.-M.; Kim, S. K.; Park, S. *Nano Lett.* **2008**, *8*, 800.
(21) Draine, B. T *Astrophys. J.* **1988**, *333*, 848.
(22) Draine, B. T.; Flatau, P. J. *J. Opt. Soc. Am. A* **1994**, *11*, 1491.
(23) Johnson, P. B.; Christy, R. W. *Phys. Rev. B* **1972**, *6*, 4370.
(24) Draine, B. T.; Goodman, J. *Astrophys. J.* **1993**, *405*, 685.
(25) Kelly, K. L.; Coronado, E.; Zhao, L. L.; Schatz, G. C. *J. Phys. Chem. B* **2003**, *107*, 668.
(26) Shuford, K. L.; Ratner, M. A.; Schatz, G. C. *J. Chem. Phys.* **2005**, *123*, 114713.
(27) Li, C.; Shuford, K. L.; Park, Q.-H.; Cai, W.; Li, Y.; Lee, E. J.; Cho, S. O. *Angew. Chem., Int. Ed.* **2007**, *46*, 3264.

NL800924R